

GNN-PMB: A Simple but Effective Online 3D Multi-Object Tracker without Bells and Whistles

Jianan Liu*, Liping Bai*, Yuxuan Xia, Tao Huang, *Senior Member, IEEE*,
Bing Zhu†, *Member, IEEE*

Abstract—Multi-object tracking (MOT) is among crucial applications in modern advanced driver assistance systems (ADAS) and autonomous driving (AD) systems. Global nearest neighbor (GNN) filter, as the earliest random vector Bayesian tracking framework, has been adopted in most of state-of-the-arts trackers and widely accepted in the automotive industry. With the development of random finite set (RFS) theory, the RFS Bayesian filters have been applied in MOT tasks recently. However, their usefulness in the real traffic for ADAS and AD application is still open to doubt. In this paper, we firstly demonstrate the latest RFS Bayesian tracking framework could be superior to typical random vector Bayesian tracking framework like GNN, via a systematic comparative study of both traditional random vector Bayesian filters with rule-based heuristic track maintenance and RFS Bayesian filters on nuScenes validation dataset. Then, we propose a RFS-based tracker, namely Poisson multi-Bernoulli filter using the global nearest neighbor (GNN-PMB), for LiDAR-based MOT tasks. This GNN-PMB tracker is simple to use but can achieve competitive results on nuScenes dataset. Specifically, the proposed GNN-PMB tracker outperforms most of the state-of-the-art LiDAR-only trackers and LiDAR and camera fusion-based trackers, ranks the 3rd among all LiDAR-only trackers on nuScenes tracking task leader board¹ at the time of submission. Our code is available at https://github.com/chisylu/gnn_pmb_tracker.

Index Terms—Multi-Object Tracking, Random Vector-based Bayesian Filters, Random Finite Set-based Bayesian Filters, GNN-PMB, LiDAR, Autonomous Driving

I. INTRODUCTION

MULTI-OBJECT tracking (MOT) is an integral and critical computational module for autonomous driving-related applications [1]. Motivations of using a multi-object tracker for MOT task include: 1) the tracker assigns and maintains a unique track ID for the same object throughout the life cycle of a tracking process; 2) the tracker rejects the false detection provided by the object detector; 3) the tracker sustains the tracking process when the tracked object fails to be detected over consecutive frames; and 4) the tracker refines the information provided by the object detector. Essentially, a multi-object tracker is a state estimator, or equivalently, a filter. In this paper, the concepts "multi-object tracker," "tracker," and "filter" are equivalent.

*Both authors contribute equally to the work and are co-first authors.

†Corresponding author.

J. Liu is with Vitalent Consulting, Gothenburg, Sweden, and Silo AI, Stockholm, Sweden. Email: jianan.liu@vitalent.se, jianan.liu@silo.ai.

L. Bai and B. Zhu are with the School of Automation Science and Electrical Engineering, Beihang University, Beijing 100191, P.R. China. Email: bai_liping@buaa.edu.cn (L. Bai); zhubing@buaa.edu.cn (B. Zhu).

Y. Xia is with Department of Electrical Engineering, Chalmers University of Technology, Gothenburg 41296, Sweden. Email: yuxuan.xia@chalmers.se.

T. Huang is with College of Science and Engineering, James Cook University, Cairns, Australia. Email: tao.huang1@jcu.edu.au.

¹<https://bit.ly/3bQJ2CP>

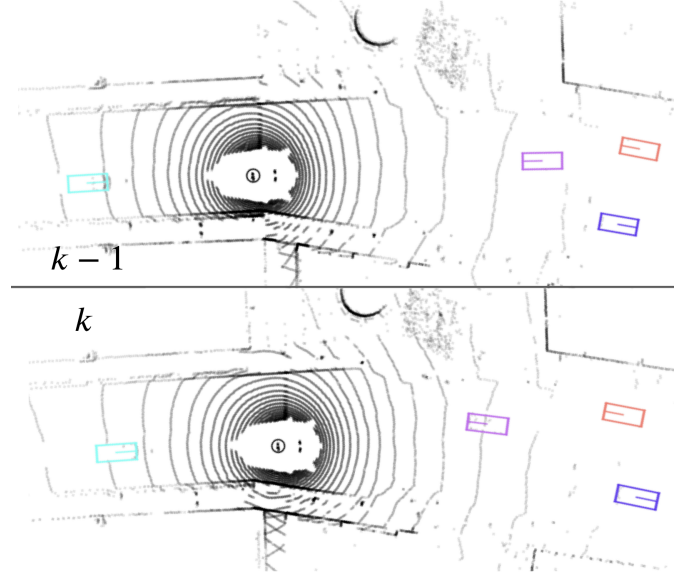


Fig. 1: Tracking-by-Detection 3D MOT using LiDAR: the outputs of the MOT filter over two consecutive frames (namely frame $k-1$ and frame k) are presented. The object surrounded by concentric circles is the ego vehicle. The grey dots are LiDAR point clouds presented in the bird-eye-view (BEV) frame. The colored bounding boxes are the projection of 3D detected bounding boxes into the BEV frame. The orientation of a bounding box is indicated by the central line with half of the length. Bounding boxes with the same color share the same track ID.

Depending on the sensor modalities employed, MOT can be categorized as 2D MOT with camera [2][3], 3D MOT with LiDAR only [1][4][5][6], and 3D MOT with both camera and LiDAR [7][8]. Base on the processing order of detection and tracking, MOT can be categorized into tracking-before-detection [9][10][11], joint-detection-and-tracking [12][13][14], and tracking-by-detection [15][16][17]. In this paper, we focus on the tracking-by-detection 3D MOT with LiDAR, which is the process when outputs of an object detector across frames are refined and connected by their corresponding track IDs, as shown by Fig. 1. Specifically, the object detector first provides the bounding box information, then the multi-object tracker refines the information provided by the object detector and assigns the appropriate ID to the bounding box.

However, the existing MOT strategies and algorithms in the literature are ever more complicated, require either additional data driven feature extraction modules or lots of tricks and rules for data association and track maintenance [18][7][8][19][20][21][22], which might not be generalized

easily in different scenarios or not be computationally feasible for embedded systems in the real-world. By contrast, this paper proposes a simple but effective online 3D multi-object tracker, namely Poisson multi-Bernoulli filter using the global nearest neighbor (GNN-PMB). The proposed GNN-PMB tracker is designed under the uniform RFS framework without requiring any feature extraction module, trick or additional rule, yet outperforms the state-of-the-art performance on the nuScenes 3D LiDAR-based MOT benchmark dataset. The main contributions of this paper are listed as follows:

- A systematic comparative study is presented for the first time by employing several commonly used Bayesian filters and the proposed GNN-PMB filter, with the different object detectors on the nuScenes benchmark dataset, according to the best of the authors' knowledge. This study is based on real-world data and provides guidelines for designing the tracking framework in practice.
- A simple but effective online LiDAR-based tracker, GNN-PMB, is proposed. The proposed GNN-PMB is designed in a unified and reasonably simple RFS framework. Such RFS framework naturally provides the solid mathematical foundations to model hypothesis management for data association and track maintenance as a whole, thus it does not require extra feature extraction module, heuristic tricks or rules for data association and track maintenance. Therefore, it is easy to tune, simple to use and more robust to detection deterioration than the GNN framework with lots of tricks and heuristics, which is widely employed by modern trackers in the practical ADAS and AD system.
- We experiment with the proposed tracker on the nuScenes dataset [23], show that the proposed LiDAR only-based tracker outperforms vast majority of the state-of-the-art trackers using LiDAR only, and is even superior to many state-of-the-art trackers using fusion of LiDAR and camera for the 3D MOT task.

The rest of the paper is arranged as follows. Section II discusses the related works of 3D LiDAR-based MOT in autonomous driving-related applications. Section III introduces the important RFSs, the modeling assumptions, and the RFS Bayesian recursion. An overview and systematic study of typical Bayesian MOT filters are presented and discussed in Section IV. The proposed GNN-PMB tracker is detailed in Section V. Experimental results are presented and analyzed in Section VI. Finally, the conclusion is drawn in Section VII.

II. RELATED WORKS

In this paper, we focused on 3D MOT with LiDAR only, which approach can be further differentiated into MOT without deep learning and MOT with deep learning. However, fusion of the data from the camera and LiDAR is another popular but more complex approach for 3D MOT. In this section, we review these approaches.

A. 3D MOT with LiDAR Only

1) *LiDAR-based 3D MOT without Deep Learning*: Weng et al. proposed AB3DMOT [1], for the LiDAR-based 3D MOT

problem. In this algorithm, the track-and-detection association is computed based on the 3D intersection over union (IoU) score [24], i.e., the track-and-detection association with the highest association score is regarded as the valid association scheme. This work establishes the baseline for the LiDAR-based 3D MOT problem by providing the code for new evaluation metrics. For example, its code is applied to evaluate the tracking challenge on the nuScenes dataset. Chui et al. proposed probabilistic 3D MOT [4] which was the first work that applied Mahalanobis distance instead of 3D IoU as the score for track-and-detection association in the 3D MOT problem. As a result, better tracking results were achieved than the AB3DMOT algorithm. SimpleTrack [5], proposed by Pang et al., uses 3D generalized intersection over union (GIoU) instead of 3D IoU as the track-and-detection score, and a non-maximum suppression (NMS) is used to process the detection information provided by the object detector. This work has demonstrated that the combination of GIoU and NMS preprocessing can improve the tracking result. ImmortalTracker [20] proposed by Wong et al., and PC3T [21] proposed by Wu et al. both evaluate the similar idea of silently maintaining the tracks even when the tracks are no longer visible. These two algorithms reduced the ID switches and fragmented tracks in tracking results. Score refinement is proposed in confidence-based 3D MOT [22] for track maintenance, where the tracker achieves a low ID switch score and track fragmentation score. Pang et al. proposed RFS-M3 [25], which firstly applies RFS-based methods, specifically PMBM filter, to the LiDAR 3D MOT problem. However, the authors did not provide implementation details and parameters. Belief Propagation Tracker, proposed by Meyer et al., formulated the MOT problem in its factor graph representation. Then, the authors employed sum-product message passing to compute the approximate marginal association probability iteratively [6]. Although the Belief Propagation Tracker did not achieve state-of-the-art performance, it was the first time messaging passing had been applied to the 3D LiDAR MOT problem.

2) *LiDAR-based 3D MOT with Deep Learning*: SimTrack [18] proposed by Luo et al. introduces an end-to-end trainable model for joint detection and tracking from raw point clouds. A graph structure is designed in OGR3MOT [26] to process detection and tracking in an online manner jointly. The graph structure is a Neural Message Passing network for fully trainable data association. Neural enhanced belief propagation (NEBP) tracker [27], proposed by Meyer et al. is an update to the Belief Propagation Tracker [6]. In the NEBP structure, the belief propagation scheme is complemented by a learned neural network. The NEBP tracker achieves superior tracking performance over its non-learning-based counterpart, namely the Belief Propagation tracker.

B. 3D MOT with LiDAR and Camera Fusion

Besides LiDAR-only approaches for 3D MOT, the fusion of LiDAR and camera is another typical strategy for 3D MOT [7][8][19]. The Probabilistic 3D Multi-Modal MOT, proposed by Chui et al., fuses features from 2D images and 3D LiDAR point clouds to capture the appearance and

geometric information of target objects [7]. The authors used a new metric that combines the Mahalanobis and feature distances for the track-and-detection association. This work showed that, by incorporating the camera information, the Probabilistic 3D Multi-Modal MOT tracker achieves better tracking results than the Probabilistic 3D multi-object tracker [4] that only uses 3D LiDAR detection as input. EagerMOT [8], proposed by Kim et al., further improves the tracking performance, compare to Probabilistic 3D Multi-Modal MOT, by utilizing the detection distance between the camera-based and the LiDAR-based detection. Zeng et al. improved the tracking performance, compare to the EagerMOT, by adding a feature extractor along with the side of the object detector in their proposed AlphaTrack algorithm [19]. The feature extractor takes image information and the LiDAR point cloud information as inputs and provides information for the track-and-detection association.

III. BASIS OF RFS-BASED METHOD

A. Set Notation

In RFS-based methods, object states (e.g., position, orientation, size of bounding box, etc.) and their corresponding measurements are represented in the form of finite sets. Assume there are n_k objects at time k . Let x_k^i denotes the state of i -th object at time k . Thus, the multi-object state at time k can be represented as a finite set $X_k = \{x_k^1, \dots, x_k^i, \dots, x_k^{n_k}\}$. The cardinality of this set is $|X_k| = n_k$. In addition, assume there are p_k measurements at time k . Let $Z_k = \{z_1, \dots, z_{p_k}\}$ denotes the set of measurements at time step k and let $Z^k = \{Z_1, \dots, Z_k\}$ denotes the sequence of all the measurement sets received so far up to and including time step k . In this paper, x_k and z_k consist of the x and y-axis information in the global coordinate.

B. Key Random Processes

Two random processes have prominent roles in the RFS-based methods: Poisson point process (PPP) and Bernoulli process. The PPP is a random set of points, such that the cardinality of the set is Poisson distributed. Similarly, the Bernoulli process is a random set of points, such that the cardinality of the set is distributed based on the Bernoulli process. X refers to the finite set, and $|X|$ refers to the cardinality of the finite set.

A PPP with intensity function $\lambda(\cdot)$ has RFS density

$$f^{\text{PPP}}(X) = e^{-\int \lambda(x)dx} \prod_{x \in X} \lambda(x), \quad (1)$$

where the intensity refers to the intensity as defined by the corresponding Poisson distribution for the cardinality distribution, and the cardinality $|X|$ is Poisson distributed with mean $\bar{\lambda} = -\int \lambda(x)dx$.

A Bernoulli process with existence probability r and existence-conditioned probability density function (PDF) $f(\cdot)$ has RFS density

$$f^{\text{ber}}(X) = \begin{cases} 1 - r & X = \emptyset; \\ rf(x) & X = \{x\}; \\ 0 & \text{otherwise.} \end{cases} \quad (2)$$

The cardinality $|X|$ is Bernoulli distributed with parameter r . For the proposed GNN-PMB tracker, the existence probability is used to indicate the likelihood of a track existence.

A multi-Bernoulli (MB) RFS X is the union of a finite number of independent Bernoulli processes X_1, \dots, X_n , and its density is

$$f^{\text{mb}}(X) = \sum_{\uplus_{i=1}^n X_i} f_i^{\text{ber}}(X_i) \quad (3)$$

where \uplus denotes the disjoint union and $f_i^{\text{ber}}(\cdot)$ is the density of the i -th Bernoulli component as shown in (2).

C. Bayesian Recursion and Multi-object Models

In Bayesian MOT filtering, the multi-object posterior $f_{k|k}(X_k|Z^k)$ is critical because it captures all the information of the multi-object state-set X_k at time step k conditioned on all the measurements. The posterior is computed by recursively applying the Chapman-Kolmogorov prediction

$$\begin{aligned} f_{k|k-1}(X_k|Z^{k-1}) \\ = \int \Phi_{k|k-1}(X_k|X_{k-1})f_{k-1|k-1}(X_{k-1}|Z^{k-1})dX_{k-1} \end{aligned} \quad (4)$$

and the Bayes update

$$f_{k|k}(X_k|Z^k) \propto G(Z_k|X_k)f_{k|k-1}(X_k|Z^{k-1}), \quad (5)$$

where $\int f(X)dX$ is the set integral [28], $\Phi_{k|k-1}(X_k|X_{k-1})$ is the multi-object transition density for modeling the dynamic motion of multiple objects, and $G(Z_k|X_k)$ is the multi-object measurement likelihood for modeling the measurement of multiple objects. In this paper, the standard multi-object dynamic model $\Phi_{k|k-1}(X_k|X_{k-1})$ is based on the following assumptions:

- Single object with state x_{k-1} at time step $k-1$ moves to a new state x_k with a Markov transition density $\phi(x_k|x_{k-1})$.
- Single object with state x_k at time step k has a probability $P^S(x_k)$ of leaving the sensor's field-of-view, where S refers to survival.
- The state of the newborn objects X_k^b at time step k appear in the sensor's field-of-view according to a PPP with intensity $\lambda_k^b(\cdot)$.
- The appearing/disappearing of newborn/existing objects and the object motions are conditionally independent of the previous multi-object state X_{k-1} .
- The set X_k of objects at time step k is the union of the set X_k^e of existing objects at time step k and the set X_k^b of newborn objects, i.e., $X_k = X_k^e \cup X_k^b$, where the superscript e refers to existing, and superscript b refers to newborn.

Specifically, the multi-object transition density from time $k-1$ to k , $\Phi_{k|k-1}(X_k|X_{k-1})$, for the proposed GNN-PMB tracker is defined by a convolution of a PPP density for newborn objects X_k^b at time time k and a multi-Bernoulli density for existing objects X_k^e inherited from time $k-1$ as following:

$$\Phi_{k|k-1}(X_k|X_{k-1}) = \sum_{X_k = X_k^b \cup X_k^c} f_k^{\text{PPP}}(X_k^b) f_{k|k-1}^{\text{mb}}(X_k^c|X_{k-1}). \quad (6)$$

The standard multi-object measurement model $G(Z_k|X_k)$ is made with the following assumptions:

- The measurement set Z_k at time step k consists of measurements Z_k^o generated by the state set X_k of objects and clutter measurements Z_k^c , i.e., $Z_k = Z_k^o \cup Z_k^c$, where the superscript o refers to the set generated by the set of objects, and the superscript c refers to the set generated by the clutter process.
- The two measurement sets Z_k^o and Z_k^c are statistically independent.
- No measurement is generated by more than one object.
- Given a state set X_k of objects, each object state $x_k \in X_k$ is either detected with probability $P^D(x_k)$, where D stand for detection probability, and generates a single measurement z_k with measurement likelihood $g(z_k|x_k)$, or misdetected with probability $1 - P^D(x_k)$.
- The measurement set Z_k^c follows a PPP with intensity $\lambda_k^c(\cdot)$.

Specifically for the proposed GNN-PMB tracker, the multi-object measurement likelihood $G(Z_k|X_k)$ is defined by a convolution of a PPP density for clutter measurements Z_k^c and a multi-Bernoulli density for object-oriented measurements Z_k^o as below:

$$G(Z_k|X_k) = \sum_{Z_k = Z_k^c \cup Z_k^o} f_k^{\text{PPP}}(Z_k^c) f_k^{\text{mb}}(Z_k^o|X_k). \quad (7)$$

IV. A SYSTEMATIC STUDY OF BAYESIAN MOT METHODS

In this section, we present a systematic comparative study of common Bayesian MOT methods from mainly two aspects: 1) track maintenance and 2) approximation methods for computational tractability.

A. Global and Local Hypotheses

The main challenge of MOT is the data association due to the unknown correspondence between objects and measurements. Therefore we start by giving a unified terminology of data association hypotheses. Consider the data associations at time step k . A local hypothesis is defined as a pair of the object-to-measurement association at time step k , and a global hypothesis is a valid collection of local hypotheses, explaining the association of every object and measurement at time step k .

To further elaborate the details of local and global hypothesis, let us consider the example illustrated in Fig. 2 (a) where there are two objects T_1, T_2 , and three measurements m_1, m_2, m_3 . The global hypotheses describing their associations are represented using binary association matrices where each entry represents a possible local hypothesis, and we use dummy notation m_0 for misdetections. Each association matrix must satisfy: 1) each column must sum to one, and 2) each row must sum to one or zero. An all-zero row, except

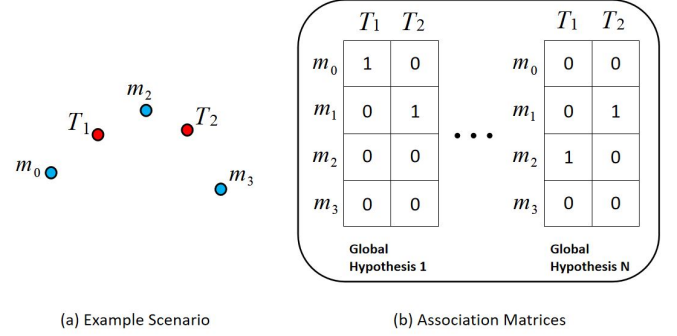


Fig. 2: An example illustrating the local and global hypotheses. Given the objects (denoted by T) and measurements (denoted by m) in (a), examples of global hypotheses, represented using association matrices are shown in (b). The 1 and 0 in the association matrix indicates whether the local hypothesis exists. 0 means the measurement is not associated with the target, and 1 otherwise.

for m_0 , means that the corresponding measurement belongs to the clutter. For the two global hypotheses shown in Fig. 2 (b), Global hypothesis 1 represents that object T_1 is misdetected and object T_2 is associated with measurement m_1 , whereas Global hypothesis N represents that object T_1 is associated to measurement m_2 and object T_2 is associated to measurement m_1 .

B. Different Bayesian MOT Methods

Bayesian MOT methods can be generally categorized into 1) MOT methods based on random vectors and 2) MOT methods based on RFSs.

1) *Vector-based MOT Methods*: Vector-based MOT methods describe the multi-object states and measurements by random vectors, and the most representative methods are the global nearest neighbor (GNN) filter [29], the joint probabilistic data association (JPDA) filter [30][31], and the multiple hypothesis tracking (MHT) filter [32].

Due to the unknown data associations, the number of global hypotheses increases hyper-exponentially over time. Therefore, the GNN filter only keeps the most likely global hypothesis at each time step. The JPDA filter first computes the (approximate) marginal object-to-measurement association probabilities and then merges local hypotheses corresponding to the same object. MHT seeks to find the most likely global hypothesis over a sliding window of consecutive time steps, which involves the propagation of multiple global hypotheses over time.

2) *Set-based MOT Methods*: Set-based MOT methods describe the multi-object states and measurements by RFSs. There are a variety of RFSs-based MOT methods in the literature. Early developments include methods that avoid explicitly handling the data association uncertainty, such as the probability hypothesis density (PHD) filter [33] and the cardinalized PHD (CPHD) filter [34] using moment approximations.

The PHD and CPHD filters approximate the multi-object posterior by a PPP and an i.i.d. cluster process, respectively,

both in the sense of minimizing the Kullback-Leibler divergence. The CPHD filter is computationally heavier than the PHD filter, but it yields better performance when the signal-to-noise ratio is low.

A significant trend in RFSs-based MOT is the development of filters based on multi-object conjugate priors, which means that the multi-object posterior has the same functional form as the predicted distribution (and the prior). A typical example is the Poisson multi-Bernoulli mixture (PMBM) filter [35], which gives the close-form solution for the standard multi-object models introduced in Section III-C. In the PMBM filter, both the prediction and the update preserve the PMBM form of the density without approximation:

$$f_{k|k'}^{\text{pmbm}}(X_k|Z^{k'}) = \sum_{X_k^u \cup X_k^d = X_k} f_{k|k'}^{\text{PPP}}(X_k^u) f_{k|k'}^{\text{mbm}}(X_k^d), \quad (8)$$

$$f_{k|k'}^{\text{mbm}}(X_k^d) = \sum_{h=1}^{H_{k'}} w_{k'}^h f_{k|k'}^h(X_k^d) \quad (9)$$

where $k' \in \{k-1, k\}$. In (8), the set $X_{k'}^u$ of undetected objects that have not yet been detected is described by a PPP, whereas the set $X_{k'}^d$ of detected objects that have been detected at least once is described by a multi-Bernoulli mixture (MBM). In the MBM (9), each multi-Bernoulli component corresponds to a unique global hypothesis for the detected objects. The h -th multi-Bernoulli component has density $f_{k|k'}^h(\cdot)$ and weight $w_{k'}^h$, which satisfies that $\sum_{h=1}^{H_{k'}} w_{k'}^h = 1$. If there is only a single multi-Bernoulli component in (9), i.e., when $H_{k'} = 1$, then the PMBM filter reduces to a PMB filter [36].

C. Track Maintenance

For practical implementations of Bayesian MOT methods, an efficient track maintenance scheme is required for tracking a time-varying number of objects. In this paper, a track is defined as a sequence of local hypothesis densities at consecutive time steps that correspond to the same object. Track maintenance refers to the process where a track is initiated, sustained, and terminated. In what follows, we discuss the track maintenance scheme for vector-based and set-based MOT methods separately.

1) *Vector-based MOT Methods*: Vector-based MOT methods can maintain track continuity by associating an object state estimate with a previous state estimate. However, they mainly rely on heuristic methods to consider the appearance/disappearance of new/existing objects. A commonly used rule for track maintenance is called *M/N* logic. Specifically, a tentative track is initiated when a measurement is not associated with existing tracks. This tentative track is confirmed if there are M measurement associations out of N consecutive time steps. The termination of tracks follows a similar procedure. Alternatively, one can use track-score-based logic for track maintenance by performing hypothesis tests.

2) *Set-based MOT Methods*: The RFS formalism facilitates modeling the appearance/disappearance of new/existing objects in a Bayesian setting. For example, in the PMBM and PMB filters, we only extract object state estimates from

Bernoulli components with existence probability above a certain threshold. However, in RFS-based MOT methods, time sequences of tracks cannot be constructed easily as the multi-object states are order-independent. One approach to maintaining track continuity is to add unique labels to the object states and form tracks by linking object state estimates with the same label [37]. A more appealing approach to solve the track-building problem is by computing multi-object densities on sets of trajectories [38], and a typical example is trajectory PMBM filter [39]. We note that the prediction and update in the PMBM filter can be an efficient method for calculating the time marginals of the RFS of trajectories [39]. Therefore, track continuity in the PMBM and PMB filters can be established using metadata. The detailed procedure is described in Section V-B2.

D. Approximations for Computational Tractability

Practical MOT implementations need efficient approximations to keep the computational complexity at a tractable level. The approximations methods can be categorized into local and global hypothesis reductions.

1) *Local Hypothesis Reduction*: The commonly used strategy to limit the number of local hypotheses is gating. Specifically, for a predicted local hypothesis density, only the associations of measurements inside its gated region require consideration to reduce the number of updated local hypotheses. In addition, different MOT methods use diverse techniques to reduce the number of local hypotheses further after the update. For example, in MHT, the number of local hypotheses is limited by implementing *N*-scan pruning [40] or by pruning local hypotheses with low scores. In Gaussian implementations of PHD and CPHD filters, Gaussian mixture reduction is performed for the PPP intensity by pruning components with small weights and merging similar components. In PMBM and PMB filters, it is necessary to prune Gaussian components in the PPP intensity with small weights and Bernoulli components with small existence probabilities.

2) *Global Hypothesis Reduction*: The key to global hypothesis reduction relies on how to solve the data association problem efficiently. For cracking the multi-scan data association problem, typical solutions include Lagrangian relaxation [40] and Markov chain Monte Carlo sampling [41]. For MOT methods considering the single-scan data association problem, the most likely global hypothesis can be obtained by solving a 2D assignment problem using algorithms such as the Hungarian algorithm [42]. The K best global hypotheses can be obtained using Murty's algorithm [42]. The merging step in the JPDA filter and the track-oriented PMB (TO-PMB) filter uses the (approximate) marginal association probabilities. They can be computed using the K best global hypotheses obtained from Murty's algorithm or directly obtained using loopy belief propagation (LBP) [43] without explicit enumeration of global hypotheses.

V. THE NEW GNN-PMB TRACKER

According to the analysis presented by [44] [45], the PMBM filter results in the best performance in simulation, but it is

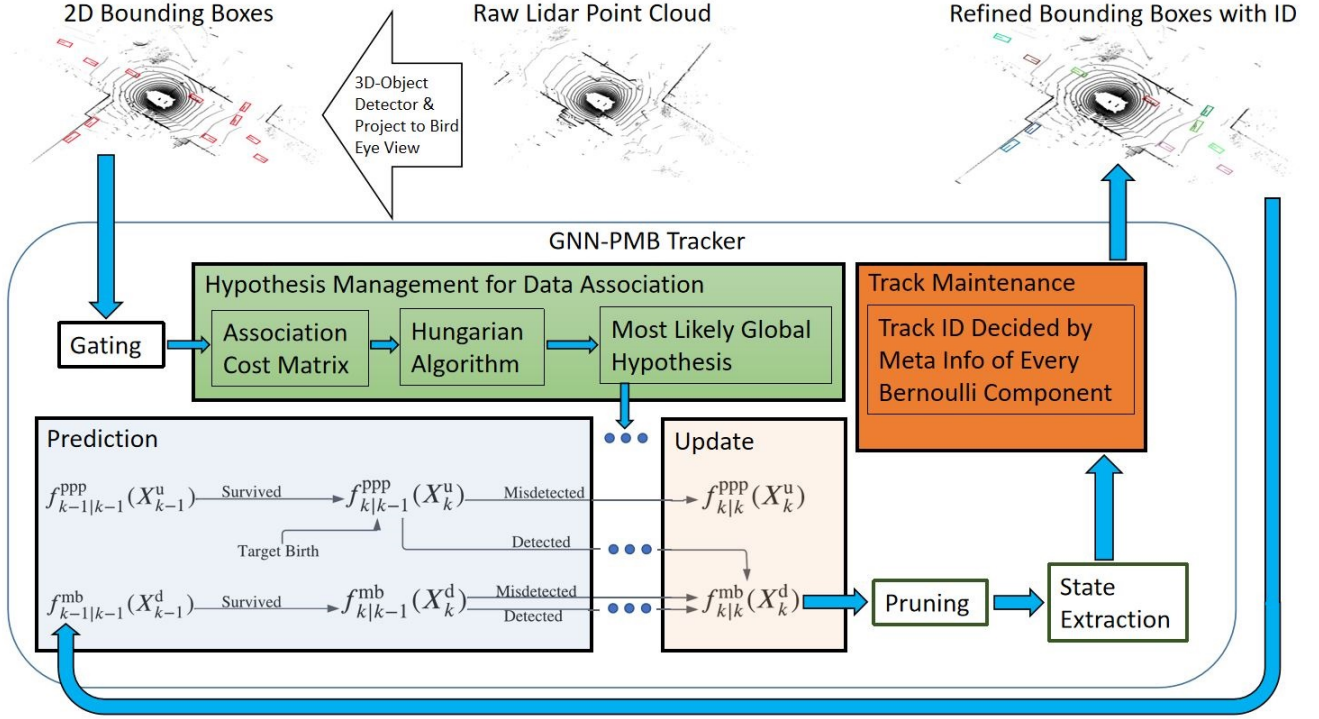


Fig. 3: The illustration of entire pipeline of GNN-PMB tracker, which consists of the recursion of PPP and the recursion of MB, hypothesis management, pruning, state extraction, and track maintenance.

computationally intensive. Thus, PMBM may not handle the real-world scenario due to existence of many objects and the corresponding measurements per frame, and the management of massive hypotheses.

There are two approaches to reducing the computational burden introduced in the hypothesis management part of the PMBM filter. The first approach is to only propagate the approximated global hypothesis by using messaging passing by employing the TO-PMB filter [36]. However, the messaging passing step is still computationally demanding. The second one is only to propagate the most likely global hypothesis. In this case, the PMBM recursion is reduced as PMB recursion with much lower computations. In this paper, we adopt the second approach and propose the GNN-PMB tracker for LiDAR-based 3D MOT correspondingly, as our proposed hypothesis management step is similar to the GNN filter. In the following of this section, we would firstly explain the overall pipeline of the proposed GNN-PMB tracker, as illustrated in Fig. 3. Then the details of two core modules, hypothesis management and track maintenance would be elaborated. The rest of the modules and corresponding parameters are discussed in the last subsection.

A. The Pipeline of GNN-PMB Tracker

Although the available information of the 3D bounding boxes provided by the LiDAR object detector includes (x, y, z) coordinate in the global frame, bounding box size, orientation, velocity, detection score, and class type information, the proposed tracker only requires the x and y coordinate in the global frame as input to keep the tracker as simple

as possible. Other information provided by the 3D LiDAR object detector is propagated without filtering. As shown in Fig. 3, the 2D bounding boxes in BEV, as the measurements of possible objects, would be utilized as input to the tracker. After the gating, the most likely global hypothesis is decided in hypothesis management procedure, by applying Hungarian algorithm for the association cost matrix which is formed using input 2D bounding boxes and prediction of detected PPPs and MBs. Then the update of PPPs and MBs is performed by standard Kalman filter according to the most likely global hypothesis, pruning and state extraction from MBs are implemented afterward to refine the objects' state. In the last, the ID information of every object is estimated to generate the trajectories.

B. Hypothesis Management and Track Maintenance for GNN-PMB Tracker

1) *Hypothesis Management*: The hypothesis management procedure, illustrated in Fig. 4, is one of the core modules for the proposed GNN-PMB tracker. A cost matrix is formed with the most likely global hypothesis at time $k - 1$, with each element representing the cost of every local hypothesis, denoted by the negative logarithm of the association likelihood score. The association likelihood score, which denotes the occurrence likelihood of a local hypothesis between a detection output and an object, is applied to organize the cost matrix for hypothesis management. In the proposed GNN-PMB filter, the association likelihood score for a local hypothesis, w , is defined as its multivariate Gaussian distribution, given by

$$\text{MVG}(z, m, \mathbf{P}) = \frac{1}{2\pi} |\mathbf{P}|^{-\frac{1}{2}} \exp^{-\frac{1}{2}(z-T)^T \mathbf{P}^{-1}(z-T)} \quad (10)$$

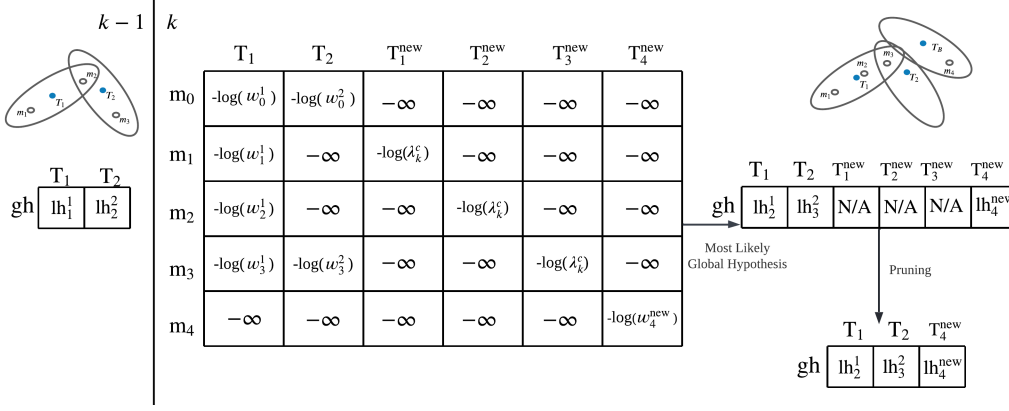


Fig. 4: The hypothesis management procedure of GNN-PMB tracker. A cost matrix is generated based on the most likely global hypothesis at time step $k - 1$ and then propagated to the current frame at time step k . At frame k , the cost matrix is organized by setting every cost element for local hypotheses within the gated area as a negative logarithm of the association likelihood score of that local hypothesis and the cost element for local hypotheses outside the gated area as infinity. Then the most likely global hypothesis at frame k is selected based on this cost matrix. In this figure, lh_m^t denotes the local hypothesis with measurement m and object t , gh stands for global hypothesis, $\lambda_k^c(\cdot)$ is the clutter intensity, and w is the likelihood score of the local hypothesis.

where z is the 2D position of detection, and T is the 2D position of a track. \mathbf{P} is the covariance matrix of the distribution of T . The cost matrix is then subjected to the Hungarian algorithm, which selects the most likely global hypothesis at time step k .

2) *Track Maintenance*: As another critical module of the proposed GNN-PMB tracker, track maintenance is implemented using meta-data maintained by every Bernoulli component. Suppose a measurement is assigned to its corresponding new Bernoulli component instead of an existing one. In that case, the new Bernoulli component would be output as a valid object, and the object ID is calculated by adding one to the current maximum ID. The new ID is stored as metadata to the new Bernoulli component. For the situation that measurement is associated with an existing Bernoulli component in the most likely global hypothesis, the Bernoulli component would be output as an existing object, and the ID of the object remains the same as the one for the existing Bernoulli component.

C. Fixed Parameters for the GNN-PMB Tracker

We categorize the parameter of the proposed GNN-PMB tracker into fixed parameter and tunable parameters. The fix parameters are set with either experience or previous work. In this subsection, we describe the fixed parameters in detail.

1) *Gating Distance*: Gating, which prunes away all the detected bounding boxes with a distance to the centeriod point of predicted tracks smaller than a threshold, before organizing the possible local hypotheses for each track. The gating distance can be defined using different metrics, e.g., Euclidean distance, 2D IoU, 2D GIoU, 2D Mahalanobis distance, etc. In the proposed GNN-PMB, we choose the 2D Mahalanobis distance which incorporates the uncertainty information as the gating distance. It is easier to compute than the 2D IoU and the 2D GIoU. It is defined by

$$d = \sqrt{(z_1 - z_2)^T \mathbf{P}^{-1} (z_1 - z_2)}, \quad (11)$$

where z_1 and z_2 are two points from the same distribution with covariance matrix \mathbf{P} . The gating threshold for the proposed GNN-PMB filter is set to be $\sqrt{50}$ in 2D Mahalanobis distance. The value is set based on the machine memory availability. For a computational device with less memory, the value can be adjusted to a smaller number.

2) *Clutter Rate*: The clutter generation process is a PPP with intensity $\lambda_k^c(\cdot)$, as discussed in Section III-C. To keep the computation as simple as possible, it is assumed that a constant expected number of clutter would be generated uniformly across the FoV. Therefore, the clutter intensity is defined as the expected number of clutters over the area of FoV. For the proposed GNN-PMB tracker, the clutter rate is set to be 0.001 over the area of FoV.

3) *Survival Probability*: As specified in Section III-C, the survival probability of an object, $P^S(x_k)$, representing how likely an object will remain for the next frame. Correspondingly, disappearance of an object can be expressed as an i.i.d Markov processes with probability $1 - P^S(x_k)$. Theoretically, the $P^S(x_k)$ should be defined in terms of the position of object x_k . For instance, the disappearance of an object is most likely to occur around the peripheries of the field of view (FoV). However, $P^S(x_k)$ is set to be a uniform P_s in order to keep the computation as simple as possible. In this paper, the P_s of the proposed GNN-PMB tracker is set to be 0.7.

4) *Probability of Detection*: Also according to Section III-C, the probability of detection of a given object x is denoted by $P^D(x_k)$, and the probability of misdetection of a given object x is denoted by $1 - P^D(x_k)$. To better capture the likelihood of every detected bounding box in the dynamic environment, $P^D(x_k)$ is specifically chosen as detection score of each detected bounding box provided by object detector, rather than being set as a constant value.

5) *Pruning Threshold of Existence Probability*: As explained in III-B, a Bernoulli process which stands for existing object is characterised by an existence probability r and existence-conditioned PDF $f(\cdot)$. To lower the computational

demand, all the Bernoulli components with an existence probability lower than the pruning threshold need to be eliminated. The pruning threshold of existence probability is set to be $1e-5$ for proposed GNN-PMB tracker, since the threshold should be small enough to retain the Bernoulli components for multiple frames before it is discarded.

D. Tunable Parameters for the GNN-PMB Tracker

The tunable parameters will be introduced here, and the relevant ablation study is presented in Section VI-C.

1) *Detection Score Threshold*: The detection score threshold is a predetermined threshold to prune the input of the tracker. For instance, a detection score threshold of 0.5 means only detected bounding boxes with a detection score higher than 0.5 would be used as input to the MOT tracker.

2) *Non-maximum Suppression (NMS) Threshold*: The object detector often creates multiple bounding boxes around the same object, but only one detection is required for each object. Non-max suppression is used to suppress the less likely bounding boxes. The NMS score is implemented as the 3D-IoU [24] score in the proposed GNN-PMB. If there are multiple bounding boxes whose 3D-IoU score exceeds the specified NMS threshold, only the bounding boxes with the highest detection score would be kept as the input to the tracker.

3) *Poisson Birth Density*: The object birth process is also modeled by PPP, as introduced in Section III-C. The cardinality is distributed according to a Poisson distribution with intensity $\lambda_k^b(\cdot)$. In the proposed GNN-PMB, $\lambda_k^b(\cdot)$ is implemented as an unnormalized Gaussian mixture with identical weight, and the initial covariance matrix P_0 is identical for all the Gaussian components. Therefore, the weight of the Gaussian distribution and the initial covariance matrix P_0 need to be tuned to specify the Poisson birth density.

4) *State Extraction Threshold*: As described in III-C, the detected multi-object state is modeled by MB RFS density for the proposed GNN-PMB tracker. Each Bernoulli RFS density has its corresponding existence probability. Only the Bernoulli components with an existence probability higher than the specified extraction threshold are considered valid objects for a given frame. Bernoulli RFS density with an existence probability lower than the specified extraction threshold would be silently maintained until the existence probability falls below the pruning threshold.

VI. EXPERIMENTS AND ANALYSIS

A. Dataset and Evaluation Metrics

There are four major LiDAR-based 3D detection and tracking benchmark datasets, namely KITTI [46], Waymo [47], nuScenes [23], and Argoverse [48]. In this work, we select the nuScenes benchmark dataset to conduct experiments as the popular nuScenes dataset provides the most reliable perception situation and large amount of testing data in the diverse scenarios for 3D MOT. To evaluate our proposed GNN-PMB properly, the basic evaluation metrics for 3D MOT on nuScenes dataset are used as the followings: Number of true positive (TP), number of false negative (FN), number of false

positive (FP), number of ID switch (IDS), and number of times a trajectory is fragmented (FRAG). In addition, number of mostly tracked (MT) tracks which denotes the number of ground-truth trajectories that are tracked for at least 80% of their respective life span, and number of mostly lost (ML) tracks which denotes the number of ground-truth trajectories that are tracked only for at most 20% of their respective life span, are also applied to provide overall evaluation. Moreover, more comprehensive metrics like average multi-object tracking accuracy (AMOTA) and the corresponding accuracy measurement multi-object tracking precision (AMOTP) are also employed in paper. The detailed information of all the metrics mentioned above can be found on the nuScenes 3D MOT challenge website².

B. Comparisons among Different Bayesian Filters

In this section, the filter performance, as shown in TABLE I, is discussed. All the secondary metrics, i.e., MT, ML, TP, FP, FN, IDS, FRAG, are evaluated under the recall with the highest MOTA score.

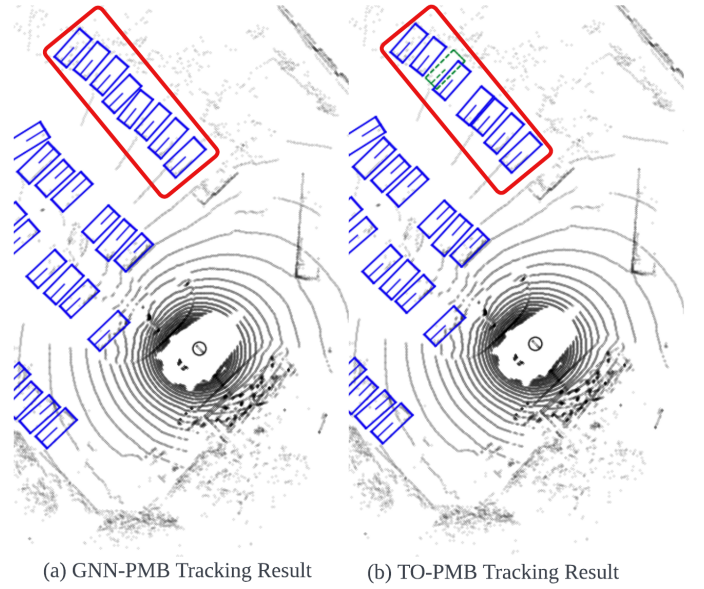


Fig. 5: The coalescence of the TP-PMB filter. This figure demonstrates the coalescence problem of the TO-PMB filter by comparing the tracking result of the same frame from both the GNN-PMB tracker and the TO-PMB tracker, where the grey dots are the LiDAR point cloud, the blue bounding boxes are the TP object, and the green bounding box with dashed line is the FN object, i.e., the object indeed exists but has not been tracked. In highlighted red rectangle area, GNN-PMB tracks all the objects correctly but TO-PMB misses one object and merges two objects into one.

1) *Quality of Detection Input*: It is critical to understand how the tracking performance would change with detector input of varying qualities. To this end, the detection files provided by three different object detectors are used in the experiment. According to the nuScenes LiDAR-based detection challenge leaderboard, the performance of the CenterPoint detector, the Megvii detector and the PointPillars detector are

²<https://www.nuscenes.org/tracking>

TABLE I: Tracking Results of Different LiDAR based Object Detectors and Bayesian Tracker Frameworks on nuScenes Validation Set.

Tracker	Detector	AMOTA \uparrow	AMOTP \downarrow	MT \uparrow	ML \downarrow	TP \uparrow	FP \downarrow	FN \downarrow	IDS \downarrow	FRAG \downarrow
GNN	PointPillars	0.251	1.403	1924	2158	50631	11776	45334	5932	2579
	Megvii	0.509	0.881	3323	1722	67774	10759	29703	4420	1209
	CenterPoint	0.603	0.735	3725	1447	72192	11767	25076	4629	1236
PHD	PointPillars	0.17	1.472	1443	2581	35583	42811	52241	14073	4728
	Megvii	0.268	1.201	478	4670	17298	6501	79652	4947	3365
	CenterPoint	0.313	1.114	835	3403	18856	39724	67996	15045	6071
TO-PMB	PointPillars	0.185	1.380	2474	2232	56685	19096	44444	768	857
	Megvii	0.294	0.926	2429	3162	49827	18613	51722	348	403
	CenterPoint	0.324	0.812	2737	2955	53982	15382	47433	482	449
PMBM	PointPillars	0.269	1.260	2709	2311	59250	12060	40800	1847	843
	Megvii	0.577	0.739	4314	1528	79094	13536	21829	974	406
	CenterPoint	0.645	0.600	4591	1349	82480	14608	18234	1183	403
GNN-PMB	PointPillars	0.311	1.231	2754	2236	60929	9993	39945	1023	769
	Megvii	0.619	0.716	4314	1552	79434	11710	21955	508	372
	CenterPoint	0.707	0.560	4608	1347	83134	12362	18113	650	345

\uparrow The upper arrow indicates that better performance is registered with higher score, same for the following tables.

\downarrow The lower arrow indicates that better performance is registered with lower score, same for the following tables.

Note: JPDA and CPHD trackers have also been implemented, but cannot be executed in real-time due that massive number of detection provided by nuScenes dataset strain JPDA and CPHD computation.

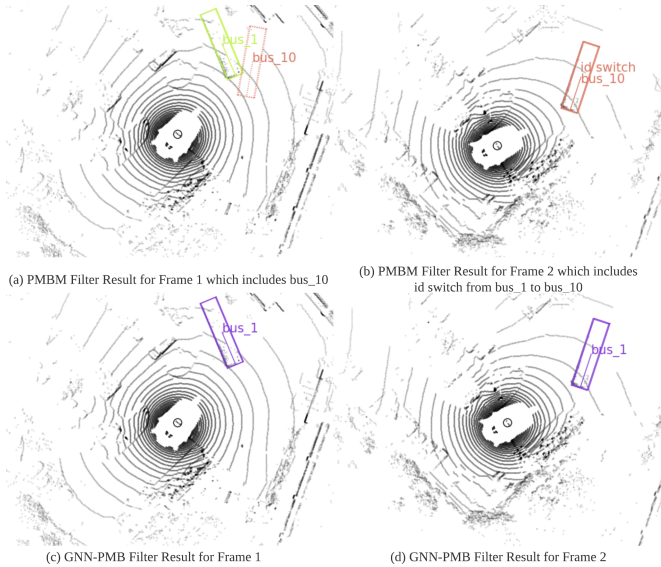


Fig. 6: Cascading failure of the PMBM filter. This figure compares the tracking result between the PMBM filter and the GNN-PMB filter. In subfigure (a), bus₁₀ represented in dash bounding box is actual a false alarm track. The track of bus₁₀ is sustained by the PMBM filter, thus leading to an ID switch where the ID of the valid track changed from bus₁ to bus₁₀ in the later frame, as illustrated in subfigure (b). These two errors are a series of cascading failures because the PMBM filter propagates K best global hypotheses. In the GNN-PMB filter, however, only the valid track for bus₁ is registered, and correctly maintained the same track ID for bus₁ in the following frame, as illustrated by subfigure (c) and (d).

in a descending order. The CenterPoint³ detection result is provided by its authors, and the challenge organizer provides the results for PointPillars⁴ and Megvii⁵. As shown by TABLE I, the tracking performances are commensurate to the quality of the detection input for all the evaluated trackers. The best

performance is achieved with the CenterPoint detector input for each tested tracker, and the worst performance is achieved with the PointPillars detector.

2) Performance of GNN, JPDA, PHD and CPHD Filter:

As shown in TABLE I, GNN filter outperforms PHD filter by a large margin despite using only simple hypothesis management for data association and heuristic rules for track maintenance, since PHD filter does not use the proper approach for data association, which may not be suitable for the situation in the real-world LiDAR-based 3D MOT.

In principle, the JPDA and CPHD filters may boost performance when compared to GNN and PHD, respectively. However, the marginal association probability computation of JPDA [32] is NP-hard and the cardinality distribution computation of CPHD has $\mathcal{O}(n_k^3)$ complexity, where n_k is the cardinality of the multi-object state at time k , the computation requirements cannot be reached due to the enormous number of detection inputs offered by the nuScenes dataset. Due to memory constraints, both filters would be automatically terminated during the tracking process.

3) *Coalescences of the TO-PMB Filter:* TABLE I also shows that the performance of TO-PMB in our experiments is insufficient. One of the reasons is that the TO-PMB would suffer from the coalescence problem, which refers to the phenomenon that multiple tracked objects are merged into one tracked object when multiple objects move in close proximity. This effect is demonstrated by Fig. 5, which is taken from a scene where the vehicle goes through a parking lot with tightly parked vehicles. In this particular frame, there should have 8 parked cars in the studied area, but the TO-PMB filter only tracked 7 parked cars as it merged two cars into one.

4) *Cascading Failure of PMBM Filter:* As the filter which achieves the second best performance in TABLE I, PMBM outperforms all other filters but still has an AMOTA score of 8.769% lower than that of the GNN-PMB with the CenterPoint detector. The performance disparity can be attributed to the fact that faulty local hypotheses would persist for the PMBM

³<https://bit.ly/3bWHSWA>

⁴<https://www.nuScenes.org/data/detection-pointpillars.zip>

⁵<https://www.nuScenes.org/data/detection-megvii.zip>

TABLE II: Ablation Study of Filter Parameters. This table indicate how the tracking result changes with different parameters.

Parameters		Value	AMOTA \uparrow	AMOTP \downarrow	RECALL \uparrow	MT \uparrow	ML \downarrow	TP \uparrow	FP \downarrow	FN \downarrow	IDS \downarrow	FRAG \downarrow
Detection Score Threshold		0.1	0.707	0.559	0.738	4606	1353	83088	12300	18167	642	341
		0.2	0.672	0.705	0.693	4391	1414	80971	9198	20318	608	328
		0.3	0.625	0.834	0.659	4266	1199	80601	9965	20564	732	500
NMS Threshold		0.1	0.707	0.560	0.730	4611	1329	83057	12491	18082	758	333
		0.98	0.680	0.572	0.715	4513	1424	81830	13240	19267	800	333
Poisson Birth Density	Weight of Gaussian Components	0.0001	0.626	0.764	0.653	4415	1588	81039	14055	20254	604	429
		0.001	0.702	0.555	0.729	4510	1533	82235	14171	19101	561	351
		0.01	0.703	0.559	0.729	4618	1383	83128	13714	18202	567	334
	Initial Covariance	0.1	0.707	0.560	0.730	4611	1329	83057	12491	18082	758	333
		15	0.699	0.566	0.730	4494	1518	81942	13036	19386	569	291
State Extraction Threshold		100	0.625	0.761	0.636	4363	1646	80024	13538	21169	704	366
		0.5	0.680	0.565	0.714	4432	1539	81294	12754	19993	610	265
		0.7	0.688	0.561	0.728	4452	1536	81625	12125	19691	581	287
		0.9	0.698	0.565	0.733	4495	1487	82057	11913	19192	648	295

filter. In contrast, the unlikely associations would not be propagated by the GNN-PMB filter, as demonstrated by Fig. 6. The figure compares the tracking result between the PMBM filter and the GNN-PMB filter. The ground truth is that there is only one track, bus1. However, the PMBM filter erroneously predicted the existence of another track bus10. Only only the PMBM made a mistake in the first frame, and the error actually persisted to later frames and resulted in an ID switch.

C. Ablation Study of Parameters for GNN-PMB Tracker

The performance of the proposed GNN-PMB tracker can be adjusted by turning the parameters described in Section V-D. A set of carefully selected parameters can let the GNN-PMB achieves a reasonably good performance. In this section, we present the ablation study of the parameter tuning process with the results shown in TABLE II.

1) *Detection Score Threshold*: The first row of TABLE II indicates that discarding the bounding box with a pre-determined detection score threshold would result in a lower AMOTA score. When the detection score threshold is set to be 0.1, 0.2, 0.3, the AMOTA score are 0.707, 0.672 and 0.625 respective. Most noticeably, the recall decreases, and the fragmented trajectories increase as the detection score threshold increases.

The TP score of the three detection thresholds are 83088, 80971, and 80601, respectively. It means there are 2117 valid detection with detection score between 0.1 and 0.2. There are 370 valid detection with detection score between 0.2 and 0.3. As the change of detection score threshold, the number of fragmented trajectories vary as well. Specifically, the fragmented trajectories increased by 172, from 328 to 500, when the detection score threshold increased from 0.2 to 0.3. It denotes that at least 172 of the 370 valid detection with detection scores between 0.2 and 0.3 are related to the id continuity of trajectories. On the contrary, the fragmented trajectories decreased by 13 from 341 to 328 when the detection score threshold increases from 0.1 to 0.2. When the detection score threshold is set to be 0.2, there are only 4391 mostly tracked trajectories, a 215 decrease from the 4606 mostly tracked trajectories when the threshold is set to be 0.1. Therefore, the decrease in fragmented trajectory is an artifact that fewer mostly tracked trajectories exist.

Our experiment result suggests that crucial information for trajectory continuity is contained in detection with a detection score lower than 0.3. Trajectory continuity is essential to later modules such as trajectory prediction and motion planning. Our observation shows that rather than applying the law of parsimony and pruning the detection with a low detection score, the output of the LiDAR 3D object detector should be provided to the MOT tracker in its entirety.

2) *NMS Threshold*: We are setting the NMS threshold to 0.1, which discards the majority of overlapping detected bounding boxes even if only a small overlap occurs, yielding an AMOTA score of 0.707 with CenterPoint as the object detector. In contrast, since keeping almost all the overlapped detected bounding boxes as input of the GNN-PMB tracker, by setting the NMS threshold as 0.98, a lower AMOTA score of 0.68 is obtained. Our observation that a basic NMS preprocess operation can achieve an AMOTA scoring difference of 0.27 denotes that only the detected bounding boxes have the least overlap with each other and should be used as input to the tracker.

3) *Poisson Birth Density*: As discussed in section V-D, proper initialization of Poisson birth density is critical prior to tracking the newborn object. On the one hand, when the initial covariance of the Gaussian component rises from 15 to 100, the AMOTA score is reduced from 0.699 to 0.625, and the related AMOTP score climbs from 0.566 to 0.761. On the other hand, beware that the greater the AMOTP, the less accurate the tracker's output is. It is reasonable since as the covariance grows, the estimation uncertainty would also increase, thus leading to rapid performance degradation.

On the other hand, the weight of the Gaussian component, which is part of the intensity of the Poisson process, also plays a crucial role in tracking the newborn objects. When the weights increase, measurement is more likely to be construed as originating from a new object than an existing one since the cost of being associated with a new object would decrease. On one extreme where the weight is too large, every measurement would be interpreted as the initial detection of a new track. On the other extreme, where the weight is too small, the measurements would always be associated with existing tracks, and no new tracks would be initiated. According to the ablation study, the AMOTA decreases as the weight decreases, while

TABLE III: Tracking Results of Our Proposed Method and Different Model-Based Trackers using LiDAR on nuScenes

Method	AMOTA↑	AMOTP↓	MT↑	ML↓	TP↑	FP↓	FN↓	IDS↓	FRAG↓
AB3DMOT (IROS 2020)* [1]	0.151	1.501	1006	4428	34808	15088	75730	9027	2557
StanfordIPRL-TRI (NeurIPS Workshop 2019)* [4]	0.550	0.798	4294	2184	85399	17533	33216	950	776
RFS-M3 (ICRA 2021)* [25]	0.619	0.752	5107	1878	90872	16728	27168	1525	856
CBMOT-LiDAR (IROS 2021)* [22]	0.649	0.592	5319	1966	94916	16469	24092	557	450
SimpleTrack (Arxiv 2021)* [5]	0.668	0.550	5476	1780	95539	17514	23451	575	591
BPTracker (Proceedings of the IEEE 2018)* [6]	0.646	0.606	5186	2259	95053	18581	24358	154	221
ImmortalTracker (Arxiv 2021)* [20]	0.677	0.599	5565	1669	96584	18012	21661	320	477
GNN-PMB (2Hz, Our)*	0.678	0.560	5698	1622	97274	17071	21521	770	431
PF-MOT tracker (ICRA 2022)** [49]	0.682	N/A	N/A	N/A	N/A	N/A	N/A	N/A	N/A
GNN-PMB (2Hz, Our)**	0.707	0.560	4608	1347	83134	12362	18113	650	345

* The metrics are reported on the nuScenes test set.

** The metrics are reported on the nuScenes validation set.

TABLE IV: Tracking Results of Our Proposed Method and Different Learning based Trackers using LiDAR on nuScenes

Method	AMOTA↑	AMOTP↓	MT↑	ML↓	TP↑	FP↓	FN↓	IDS↓	FRAG↓
SimTrack (ICCV 2021)* [18]	0.645	0.681	5063	1986	92093	17443	26430	1042	472
OGR3MOT (IEEE RAL 2022)* [26]	0.656	0.620	5278	2094	95264	17877	24013	288	371
NEBP (Arxiv 2022)* [27]	0.673	0.586	5380	2126	97023	19535	22380	162	256
GNN-PMB (2Hz, Our)*	0.678	0.560	5698	1622	97274	17071	21521	770	431
TransMOT (IEEE IV 2022)** [50]	0.674	0.754	2096	N/A	N/A	9449	14071	1403	N/A
GNN-PMB (2Hz, Our)**	0.849	0.387	2762	668	49182	6140	8791	344	170

* The metrics are reported on the nuScenes test set.

** The metrics are reported on the nuScenes validation set for car.

TABLE V: Tracking Results of Our Proposed Method and Different Trackers using LiDAR and Camera Fusion on nuScenes Test Set

Method	AMOTA↑	AMOTP↓	MT↑	ML↓	TP↑	FP↓	FN↓	IDS↓	FRAG↓
Probabilistic3DMM (ICRA 2021)* [7]	0.655	0.617	5494	1557	95199	18061	23323	1043	717
EagerMOT (ICRA 2021)* [8]	0.677	0.550	5303	1842	93484	17705	24925	1156	601
CBMOT (IROS 2021)* [22]	0.676	0.518	5420	1654	96028	21604	22828	709	1015
AlphaTrack (IROS 2021)* [19]	0.693	0.585	5560	1744	95851	18421	22996	718	480
GNN-PMB (2Hz, Our)**	0.678	0.560	5698	1622	97274	17071	21521	770	431

* All trackers are based fusion of LiDAR and camera.

** Our tracker is based on LiDAR only.

the ID switch varies at a different pace as the weight varies. Consequently, such observation demonstrates that finding a suitable value for the weight of the Gaussian component to fit the statistics of object birth in the nuScenes dataset is essential.

4) *State Extraction Threshold*: Since the probability of the Bernoulli component signifies how probable an object exists, precisely selecting its extraction threshold becomes vital for the final estimation of object states. According to our ablation investigation, raising the extraction threshold increases AMOTA, MT, and TP while lowering ML, FP, and FN. This result reveals that preserving the Bernoulli components with a high enough existence probability would result in a more accurate track estimation.

D. Performance Comparison between Our GNN-PMB Tracker using LiDAR Only and Other State-Of-The-Art Methods

1) *Performance Comparison with State-of-The-Art Model-based LiDAR Trackers using LiDAR Only*: In the nuScenes test dataset, our proposed LiDAR only tracker, GNN-PMB, is compared against various model-based LiDAR only trackers in TABLE III. Among the model-based trackers, the proposed GNN-PMB tracker receives the highest AMOTA score, which

is 0.678, 4.95% percent higher than the second-best model-based tracker. Regarding AMOTP, the GNN-PMB tracker achieves a score of 0.560, which is only 0.01 lower than that of SimpleTrack, and it is the second-best AMOTP score amongst all compared model-based trackers. However, other trackers use all the 3D information provided by the object detector as input of the tracker, GNN-PMB tracker only utilizes the x and y coordinates in the global frame as input.

Our proposed method also outperforms all the model-based trackers in MT, ML, TP, and FN, with the FP score coming in second only to CBMOT-LiDAR. Notably, the GNN-PMB tracker achieves an MT score of 5698. Even with lower frequency input (i.e., 2Hz), the GNN-PMB tracker still successfully tracked 4.05% more tracks than SimpleTrack, which employed detection at 10Hz as the input. Moreover, the GNN-PMB tracker is even superior to ImmortalTracker, which is an offline smoother refines the trajectory with more accumulated information in the future, though it is impractical in the real-world system for online tracking. Another recent proposed LiDAR-only model-based tracker, the PF-MOT tracker, only reported performances partially in the nuScenes validation dataset rather than the test dataset. Thus we can only compare

it with it on the validation dataset. The result shows that the GNN-PMB tracker achieves an AMOTA of 0.707, which is also higher than the 0.682 AMOTA achieved by the PF-MOT tracker.

The drawbacks of the GNN-PMB tracker are the higher IDS and FRAG compared to BPTTracker, which has only 154 ID switches and 221 fragments. However, considering relatively low values in MT, the low ID switches achieved by the BPTTracker could be an artifact from having less mostly tracked tracks.

2) *Performance Comparison with State-Of-The-Art Data-driven Trackers using LiDAR Only:* We also compare our proposed GNN-PMB with learning-based state-of-the-art trackers. As shown by TABLE IV, our proposed GNN-PMB tracker achieves the best performance in all evaluation metrics other than IDS and FRAG when it is compared with the data-driven trackers. The NEBP tracker and the OGR3MOT Tracker have low ID switches because the BPTTracker has a low IDS score, as explained in Section VI-D1.

In particular, our proposed GNN-PMB tracker achieves an AMOTP score of 0.56, which is 0.026 better than the NEBP tracker, the second-best tracker among all the learning-based trackers. Furthermore, the AMOTP score indicates that the GNN-PMB tracker can provide more accurate position information than the NEBP tracker.

3) *Performance Comparison with State-Of-The-Art Trackers using LiDAR and Camera Fusion:* To further demonstrate the advantages of our proposed GNN-PMB tracker, we present the comparison between the proposed GNN-PMB and the state-of-the-art trackers using LiDAR and camera fusion. It is worth pointing out that, in contrast to state-of-the-art trackers utilizing LiDAR and camera fusion, our proposed GNN-PMB tracker only uses LiDAR to obtain comparable tracking performance on AMOTA and AMOTP and is even superior on MT, TP, FP, and FN, as shown in TABLE V. Such results show an enormous potential to increase performance even further when the GNN-PMB tracking framework is extended into settings with the fusion of LiDAR and camera.

VII. CONCLUSION AND FUTURE WORK

This paper shows a systematical comparison between different random vector Bayesian and RFS filters on the nuScenes validation dataset. Based on this, a simple but effective online multi-object tracker in a uniform RFS framework, GNN-PMB, which only requires the x and y coordinates of the bounding box in the global frame to be used as input, is proposed. Such a MOT scheme which is easy to use and simple to tune, achieved state-of-the-art performance on the nuScenes benchmark dataset. Thanks to the simple RFS framework, the performance of our proposed method can be potentially further improved with a simple modification, such as providing 3D state information as input, employing both LiDAR and camera as sensor modalities, and a meta-learning-based parameter auto-tuning module. For future work, downstream tasks such as trajectory prediction and motion planning should also be incorporated into the assessment of the multi-object trackers to design a more robust multi-object tracker in an end-to-end manner.

REFERENCES

- [1] X. Weng, J. Wang, D. Held, and K. Kitani, "3d multi-object tracking: A baseline and new evaluation metrics," in *2020 IEEE/RSJ International Conference on Intelligent Robots and Systems (IROS)*. IEEE, 2020, pp. 10 359–10 366.
- [2] Y. Zhang, C. Wang, X. Wang, W. Zeng, and W. Liu, "Fairmot: On the fairness of detection and re-identification in multiple object tracking," *International Journal of Computer Vision*, pp. 1–19, 2021.
- [3] Y. Zhang, P. Sun, Y. Jiang, D. Yu, Z. Yuan, P. Luo, W. Liu, and X. Wang, "Bytetrack: Multi-object tracking by associating every detection box," *arXiv preprint arXiv:2110.06864*, 2021.
- [4] H. Kuang Chiu, A. Prioletti, J. Li, and J. Bohg, "Probabilistic 3d multi-object tracking for autonomous driving," *ArXiv*, vol. abs/2001.05673, 2020.
- [5] Z. Pang, Z. Li, and N. Wang, "Simpletrack: Understanding and rethinking 3d multi-object tracking," *arXiv preprint arXiv:2111.09621*, 2021.
- [6] F. Meyer, T. Kropfreiter, J. L. Williams, R. Lau, F. Hlawatsch, P. Braca, and M. Z. Win, "Message passing algorithms for scalable multitarget tracking," *Proceedings of the IEEE*, vol. 106, no. 2, pp. 221–259, 2018.
- [7] H.-k. Chiu, J. Li, R. Ambrus, and J. Bohg, "Probabilistic 3d multi-modal, multi-object tracking for autonomous driving," in *2021 IEEE International Conference on Robotics and Automation (ICRA)*. IEEE, 2021, pp. 14 227–14 233.
- [8] A. Kim, A. Ošep, and L. Leal-Taixé, "Eagermot: 3d multi-object tracking via sensor fusion," in *2021 IEEE International Conference on Robotics and Automation (ICRA)*. IEEE, 2021, pp. 11 315–11 321.
- [9] S. J. Davey, M. G. Rutten, and B. Cheung, "A comparison of detection performance for several track-before-detect algorithms," *EURASIP Journal on Advances in Signal Processing*, vol. 2008, pp. 1–10, 2007.
- [10] D. Salmond and H. Birch, "A particle filter for track-before-detect," in *Proceedings of the 2001 American Control Conference (Cat. No. 01CH37148)*, vol. 5. IEEE, 2001, pp. 3755–3760.
- [11] S. J. Davey, M. G. Rutten, and B. Cheung, "A comparison of detection performance for several track-before-detect algorithms," *EURASIP Journal on Advances in Signal Processing*, vol. 2008, pp. 1–10, 2007.
- [12] Z. Lu, V. Rathod, R. Votel, and J. Huang, "Retinatrack: Online single stage joint detection and tracking," in *Proceedings of the IEEE/CVF conference on computer vision and pattern recognition*, 2020, pp. 14 668–14 678.
- [13] J. Czyz, B. Ristic, and B. Macq, "A particle filter for joint detection and tracking of color objects," *Image and Vision Computing*, vol. 25, no. 8, pp. 1271–1281, 2007.
- [14] B. T. Vo, C. M. See, N. Ma, and W. T. Ng, "Multi-sensor joint detection and tracking with the bernoulli filter," *IEEE Transactions on Aerospace and Electronic Systems*, vol. 48, no. 2, pp. 1385–1402, 2012.
- [15] M. D. Breitenstein, F. Reichlin, B. Leibe, E. Koller-Meier, and L. Van Gool, "Robust tracking-by-detection using a detector confidence particle filter," in *2009 IEEE 12th International Conference on Computer Vision*. IEEE, 2009, pp. 1515–1522.
- [16] E. Bochinski, V. Eiselein, and T. Sikora, "High-speed tracking-by-detection without using image information," in *2017 14th IEEE international conference on advanced video and signal based surveillance (AVSS)*. IEEE, 2017, pp. 1–6.
- [17] J. F. Henriques, R. Caseiro, P. Martins, and J. Batista, "Exploiting the circulant structure of tracking-by-detection with kernels," in *European conference on computer vision*. Springer, 2012, pp. 702–715.
- [18] C. Luo, X. Yang, and A. Yuille, "Exploring simple 3d multi-object tracking for autonomous driving," *International Conference on Computer Vision (ICCV)*, 2021.
- [19] Y. Zeng, C. Ma, M. Zhu, Z. Fan, and X. Yang, "Cross-modal

- 3d object detection and tracking for auto-driving,” in *2021 IEEE/RSJ International Conference on Intelligent Robots and Systems (IROS)*. IEEE, 2021, pp. 3850–3857.
- [20] Q. Wang, Y. Chen, Z. Pang, N. Wang, and Z. Zhang, “Immortal tracker: Tracklet never dies,” *arXiv preprint arXiv:2111.13672*, 2021.
- [21] H. Wu, W. Han, C. Wen, X. Li, and C. Wang, “3d multi-object tracking in point clouds based on prediction confidence-guided data association,” *IEEE Transactions on Intelligent Transportation Systems*, vol. 23, pp. 5668–5677, 2022.
- [22] N. Benbarka, J. Schröder, and A. Zell, “Score refinement for confidence-based 3d multi-object tracking,” *2021 IEEE/RSJ International Conference on Intelligent Robots and Systems (IROS)*, 2021.
- [23] H. Caesar, V. Bankiti, A. H. Lang, S. Vora, V. E. Liong, Q. Xu, A. Krishnan, Y. Pan, G. Baldan, and O. Beijbom, “nuScenes: A multimodal dataset for autonomous driving,” in *Proceedings of the IEEE/CVF conference on computer vision and pattern recognition*, 2020, pp. 11 621–11 631.
- [24] Z. Zheng, P. Wang, W. Liu, J. Li, R. Ye, and D. Ren, “Distance-iou loss: Faster and better learning for bounding box regression,” in *Proceedings of the AAAI conference on artificial intelligence*, vol. 34, no. 07, 2020, pp. 12 993–13 000.
- [25] S. Pang, D. Morris, and H. Radha, “3d multi-object tracking using Random Finite Set-based multiple measurement models filtering (RFS-M 3) for autonomous vehicles,” in *2021 IEEE International Conference on Robotics and Automation (ICRA)*. IEEE, 2021, pp. 13 701–13 707.
- [26] J.-N. Zaech, D. Dai, A. Liniger, M. Danelljan, and L. V. Gool, “Learnable online graph representations for 3d multi-object tracking,” *IEEE Robotics and Automation Letters*, vol. 7, pp. 5103–5110, 2022.
- [27] M. Liang and F. Meyer, “Neural enhanced belief propagation for data association in multiobject tracking,” *arXiv preprint arXiv:2203.09948*, 2022.
- [28] R. P. Mahler, *Statistical multisource-multitarget information fusion*. Artech House Norwood, MA, USA, 2007, vol. 685.
- [29] S. S. Blackman and R. Popoli, *Design and analysis of modern tracking systems*. Artech House Publishers, 1999.
- [30] T. Fortmann, Y. Bar-Shalom, and M. Scheffe, “Sonar tracking of multiple targets using joint probabilistic data association,” *IEEE journal of Oceanic Engineering*, vol. 8, no. 3, pp. 173–184, 1983.
- [31] Y. Bar-Shalom, F. Daum, and J. Huang, “The probabilistic data association filter,” *IEEE Control Systems Magazine*, vol. 29, no. 6, pp. 82–100, 2009.
- [32] D. Reid, “An algorithm for tracking multiple targets,” *IEEE transactions on Automatic Control*, vol. 24, no. 6, pp. 843–854, 1979.
- [33] B.-N. Vo and W.-K. Ma, “The Gaussian Mixture Probability Hypothesis Density Filter,” *IEEE Transactions on Signal Processing*, vol. 54, pp. 4091–4104, 2006.
- [34] B.-T. Vo, B.-N. Vo, and A. Cantoni, “The Cardinalized Probability Hypothesis Density Filter for Linear Gaussian Multi-Target Models,” *2006 40th Annual Conference on Information Sciences and Systems*, pp. 681–686, 2006.
- [35] Á. F. García-Fernández, J. L. Williams, K. Granström, and L. Svensson, “Poisson Multi-Bernoulli Mixture Filter: Direct derivation and implementation,” *IEEE Transactions on Aerospace and Electronic Systems*, vol. 54, pp. 1883–1901, 2018.
- [36] J. L. Williams, “Marginal multi-Bernoulli filters: RFS derivation of MHT, JPDA, and association-based MeMBer,” *IEEE Transactions on Aerospace and Electronic Systems*, vol. 51, no. 3, pp. 1664–1687, 2015.
- [37] K. Panta, D. E. Clark, and B.-N. Vo, “Data association and track management for the Gaussian mixture probability hypothesis density filter,” *IEEE transactions on aerospace and electronic systems*, vol. 45, no. 3, pp. 1003–1016, 2009.
- [38] Á. F. García-Fernández and L. Svensson, “Trajectory PHD and CPHD filters,” *IEEE Transactions on Signal Processing*, vol. 67, no. 22, pp. 5702–5714, 2019.
- [39] K. Granström, L. Svensson, Y. Xia, J. Williams, and Á. F. García-Fernández, “Poisson multi-Bernoulli mixture trackers: Continuity through random finite sets of trajectories,” in *2018 21st International Conference on Information Fusion (FUSION)*. IEEE, 2018, pp. 1–5.
- [40] S. S. Blackman, “Multiple Hypothesis Tracking for multiple target tracking,” *IEEE Aerospace and Electronic Systems Magazine*, vol. 19, pp. 5–18, 2004.
- [41] S. Oh, S. Russell, and S. Sastry, “Markov chain Monte Carlo data association for multi-target tracking,” *IEEE Transactions on Automatic Control*, vol. 54, no. 3, pp. 481–497, 2009.
- [42] D. F. Crouse, “On implementing 2D rectangular assignment algorithms,” *IEEE Transactions on Aerospace and Electronic Systems*, vol. 52, no. 4, pp. 1679–1696, 2016.
- [43] J. L. Williams and R. A. Lau, “Approximate evaluation of marginal association probabilities with belief propagation,” *IEEE Transactions on Aerospace and Electronic Systems*, vol. 50, pp. 2942–2959, 2014.
- [44] Y. Xia, K. Granström, L. Svensson, and Á. F. García-Fernández, “Performance evaluation of multi-Bernoulli conjugate priors for multi-target filtering,” in *2017 20th International Conference on Information Fusion (Fusion)*. IEEE, 2017, pp. 1–8.
- [45] J. Smith, F. Particke, M. Hiller, and J. Thielecke, “Systematic analysis of the PMBM, PHD, JPDA and GNN multi-target tracking filters,” in *2019 22th International Conference on Information Fusion (FUSION)*. IEEE, 2019, pp. 1–8.
- [46] A. Geiger, P. Lenz, C. Stiller, and R. Urtasun, “Vision meets robotics: The kitti dataset,” *The International Journal of Robotics Research*, vol. 32, no. 11, pp. 1231–1237, 2013.
- [47] P. Sun, H. Kretschmar, X. Dotiwalla, A. Chouard, V. Patnaik, P. Tsui, J. Guo, Y. Zhou, Y. Chai, B. Caine, *et al.*, “Scalability in perception for autonomous driving: Waymo open dataset,” in *Proceedings of the IEEE/CVF conference on computer vision and pattern recognition*, 2020, pp. 2446–2454.
- [48] M.-F. Chang, J. Lambert, P. Sangkloy, J. Singh, S. Bak, A. Hartnett, D. Wang, P. Carr, S. Lucey, D. Ramanan, *et al.*, “Argoverse: 3d tracking and forecasting with rich maps,” in *Proceedings of the IEEE/CVF Conference on Computer Vision and Pattern Recognition*, 2019, pp. 8748–8757.
- [49] N. F. Wen Tao, Yanyong Zhang, “PF-MOT: Probability fusion based 3d multi-object tracking for autonomous vehicles,” *IEEE International Conference on Robotics and Automation (ICRA)*, 2022.
- [50] F. Ruppel, F. Faion, C. Gläser, and K. Dietmayer, “Transformers for multi-object tracking on point clouds,” *IEEE Intelligent Vehicles Symposium (IV)*, 2022.